

# Multi-fractality of the entanglement Hamiltonian eigen-modes

Mohammad Pouranvari

*Department of Physics, Faculty of Basic Sciences,  
University of Mazandaran, P. O. Box 47416-95447, Babolsar, Iran*  
(Dated: March 21, 2022)

We study the fractal properties of single-particle eigen-modes of entanglement Hamiltonian in free fermion models. One of these modes that has the highest entanglement information and thus called maximally entangled mode (MEM) is specially considered. In free Fermion models with Anderson localization, fractality of MEM is obtained numerically and compared with the fractality of Hamiltonian eigen-mode at Fermi level. We show that both eigen-modes have similar fractal properties: both have same single fractal dimension in delocalized phase which equals the dimension of the system, and both show multi-fractality at phase transition point. Therefore, we conclude that, fractal behavior of MEM – in addition to the fractal behavior of Hamiltonian eigen-mode – can be used as a quantum phase transition characterization.

## I. INTRODUCTION

Quantum phase transition happens at zero temperature, where quantum fluctuations – in contrast to temperature dependent fluctuations – are dominant and drive the phase transition. These fluctuations yield to broadly distributed observable quantities at the phase transition point. Anderson transition<sup>1</sup> between delocalized and localized phases, is one example of quantum phase transition which has attracted much attention. The original Anderson phase transition was introduced as a three-dimensional ( $3d$ ) tight binding lattice model with randomness in on-site energies. For a specific value of the randomness strength, the state at the Fermi level becomes localized. In this theory the lower critical dimension is 3. In  $1d$  and  $2d$  cases, all states in the thermodynamic limit are localized for an infinitesimal amount of disorder and subsequently there is no Anderson phase transition. Later on,  $1d$  and  $2d$  models were proposed with *correlated disorder* that have delocalized-localized transition.<sup>2</sup> Anderson transition, as a quantum phase transition, exhibits statistical fluctuations at the phase transition point. These fluctuations are manifested in the anomalous scaling of the inverse participation ratio (defined below) of Hamiltonian eigen-mode at the Fermi energy  $|E_F\rangle$ , which lead to fractal behavior at the phase transition point. Such fractal behavior can be used as a tool to distinguish different phases.<sup>3</sup> Multi-fractal analysis has broad applications in different branches of science including physiology,<sup>4,5</sup> geophysics,<sup>6,7</sup> fluid dynamics,<sup>8-13</sup> and even in finance.<sup>14-18</sup>

Some early reports on the fractal behavior of the  $|E_F\rangle$  are Refs. [19–25] where its fractal properties are analyzed in different phases and used as a phase characterization. Some more recent reports are the followings: based on an analytic calculation, Ref. [26] shows that there is a symmetry in the multi-fractal spectrum of  $|E_F\rangle$ . The relation between single-particle entanglement entropy and fractal dimensions at the phase transition point was found in Refs. [27 and 28]; also Ref. [29] proves analytically and then shows numerically that multi-fractality of  $|E_F\rangle$  at the phase transition point can be obtained by using mo-

ments of Rényi entropy. Refs. [30 and 31] calculate the singularity spectrum of  $|E_F\rangle$  in Anderson  $3d$  model and compare the typical average with the ensemble average in calculation of singularity spectrum. Furthermore, in Ref. [32] singularity spectrum is obtained by calculating the probability distribution of  $|\psi_i|^2$  ( $\psi_i$  as the wave-function at site  $i$ ).

In this paper, we propose to study the problem of Anderson transition from the point of view of multi-fractality of entanglement Hamiltonian. Let us recall the definition of entanglement Hamiltonian. If the system is in state  $|\psi\rangle$ , then the density matrix will be given by  $\rho = |\psi\rangle\langle\psi|$ . For a bipartite system, reduced density matrix for one subsystem is obtained by tracing over degrees of freedom of other subsystem. As we know, for free Fermion, we can write the reduced density matrix as  $e^{-H_{ent}}$ , where the  $H_{ent}$  is a free Fermion Hamiltonian and called entanglement Hamiltonian. Entanglement Hamiltonian eigen-modes of two subsystems are then attached together to make a mode for the entire system.<sup>33</sup> The mode corresponding to smallest magnitude entanglement energy which has the largest contribution to the entanglement entropy is distinguished from others, since it has important physical information about the system.<sup>34-37</sup> This mode is called maximally entangled mode (MEM).

In Ref. [34] it is shown, regarding the localization of the mode, that MEM and  $|E_F\rangle$  contain the same physics: both are localized in the localized regime and both are extended in delocalized regime. In addition, their overlap at the phase transition point is larger than their overlap in delocalized or localized phases, although small compare to 1. Here, regarding the comparison of two modes from indirect point of view of fractality, we ask the following questions: does MEM show multi-fractality at the phase transition point? Can we use fractal behavior of MEM to distinguish different phases?

In this paper, we answer the above questions, using two  $1d$  models and the  $3d$  Anderson model. We obtain  $|E_F\rangle$  using numerically exact diagonalization of the Hamiltonian which is an  $N \times N$  matrix ( $N$  is the system size). And to obtain the MEM, we follow the method mentioned in Ref. [33] where we have to diagonalize another

matrix with dimension  $N_F \times N_F$  ( $N_F$  is the Fermion number). These two diagonalization procedures make the calculations very time consuming and thus we are limited in the system size for the case of  $3d$  Anderson model.

Our key results are as follows: In the delocalized phase, MEM, like  $|E_F\rangle$  has a single fractal dimension equal to dimension of the system  $d$ , while in the localized phase, the fractal dimension goes to zero. More importantly, at the phase transition point, MEM shows multi-fractality; we calculated numerically its multi-fractal spectrum and also show that MEM obeys the symmetry relation of anomalous exponents. Furthermore, we can distinguish different phases based on the singular spectrum of the MEM.

This paper is organized as follows: in section II we explain multi-fractality as a mathematical concept and then apply it to wave-function in lattice systems. The models we intend to study are next explained in section III. Section IV contains main results of our numerical calculations. Finally, the summary of our work is presented in section V.

## II. MULTI-FRACTALITY ANALYSIS

Suppose that we have  $\mathcal{N}$  numbers, randomly distributed. Dividing this set of numbers into cells with size  $\ell$ , the probability that a number is in the  $i$ th cell,  $p_i(\ell)$  is proportional to the numbers included in that cell  $\mathcal{N}_i$ :  $p_i(\ell) = \mathcal{N}_i/\mathcal{N}$ .

Scaling behavior of moments of the probability, averaged over all cells, tells us the multi-fractal structure of these random numbers:

$$\langle p_i(\ell)^{q-1} \rangle \propto \ell^{\tau(q)}, \quad (1)$$

where the multi-fractal spectrum is defined as below:

$$\tau(q) = (q-1)D(q). \quad (2)$$

If  $D(q)$  is independent of  $q$ , we call  $D$  the single-fractal dimension; otherwise, when  $\tau$  is not a linear function of  $q$ , we have *multi-fractality*.<sup>21</sup>

Now, in view of above method of characterizing random numbers, the fractal behavior of an eigen-function in a lattice system can be studied, where  $|\psi_i|^2$ 's for the  $i$ th lattice sites are the random numbers. We want to obtain the scaling behavior of the so called generalized inverse participation ratio(GIPR)  $P_q$ , defined below:

$$P_q(\ell) = \sum_k^{N_\ell} \mu_k^q(\ell), \quad (3)$$

$$\mu_k(\ell) = \sum_i^\ell |\psi_i|^2, \quad (4)$$

in which we divide the system with size  $N$  into  $N_\ell$  cells, each containing  $\ell$  sites and we coarse grain over cells with

Eq. (4). For a wave-function

$$P_q \sim \lambda^{\tau(q)}, \quad \text{where } \lambda = \ell/N. \quad (5)$$

The behavior of the multi-fractal spectrum  $\tau(q)$  can be used as a characterization for Anderson localization:<sup>3</sup>

$$\tau(q) \sim \begin{cases} 0, & \text{in localized phase} \\ D(q)(q-1), & \text{at the phase transition point} \\ d(q-1), & \text{in delocalized phase} \end{cases} \quad (6)$$

i.e. in the localized phase no scaling behavior is seen. In the delocalized phase, the singularity spectrum  $\tau$  is a linear function of  $q$  with a constant slope of  $d$  and thus the wave-function is considered to have *single-fractal* dimension. On the other hand, at the phase transition point,  $\tau(q)$  is a non-linear function of  $q$  with a varying slope of  $D(q)$  and the wave-function is *multi-fractal*.

In addition,  $\tau(q)$  is written as:

$$\tau(q) = d(q-1) + \Delta_q, \quad (7)$$

where  $\Delta_q$  are the anomalous exponents that are zero in the delocalized phase and hold the following symmetry relation at the phase transition point:<sup>26</sup>

$$\Delta_q = \Delta_{1-q}. \quad (8)$$

By applying Legendre transformation, one obtains the singularity spectrum  $f(\alpha)$ :

$$\alpha = \frac{d\tau(q)}{dq}, \quad (9)$$

$$f(\alpha) = q \frac{d\tau}{dq} - \tau. \quad (10)$$

$f(\alpha)$  is the *fractal* dimension of points where  $|\psi_i|^2 = N^{-\alpha}$ , i.e. number of such points that scale as  $N^{f(\alpha)}$ .

## III. MODELS

The first model we study is the Aubry-Andre (AA) model.<sup>38</sup> It is a  $1d$  tight binding model with the Hamiltonian:

$$H = -t \sum_{\langle i,j \rangle} (c_i^\dagger c_j + c_j^\dagger c_i) + \sum_i \epsilon_i c_i^\dagger c_i, \quad (11)$$

where  $c_i^\dagger(c_i)$  is the creation (annihilation) operator for the site  $i$  in the second quantization representation and  $\langle \rangle$  indicates nearest neighbor hopping only. Hopping amplitudes are constant  $t = 1$ , and on-site energy  $\epsilon_i$  at site  $i$  has an incommensurate period:

$$\epsilon_i = 2\eta \cos(2\pi i b), \quad (12)$$

where  $b = \frac{1+\sqrt{5}}{2}$  is the golden ratio. This model has a phase transition at  $\eta = 1$ . As we change  $\eta$ , we go

through a phase transition from delocalized states ( $\eta < 1$ ) to localized states ( $\eta > 1$ ).

Another model is power-law bond disordered Anderson model (PRBA)<sup>39</sup> which is a  $1d$  model with the Hamiltonian:

$$H = \sum_{i,j=1}^N h_{ij} c_i^\dagger c_j \quad (13)$$

in which on-site energies are zero, and long-range hopping amplitudes are

$$h_{ij} = w_{ij}/|i-j|^a \quad (14)$$

where  $w$ 's are uniformly random numbers distributed between  $-1$  and  $1$ . There is a phase transition at  $a = 1$  between delocalized state ( $a < 1$ ) and localized state ( $a > 1$ ). The other model is power-law random banded matrix model (PRBM)<sup>40</sup> which is a  $1d$  long range hopping model with the Hamiltonian of Eq. (13): matrix elements  $h_{ij}$  are random numbers, distributed by a Gaussian distribution function that has zero mean and the following variance (with periodic boundary condition):

$$\langle |h_{ij}|^2 \rangle = \left[ 1 + \left( \frac{\sin \pi(i-j)/N}{b\pi/N} \right)^{2a} \right]^{-1}, \quad (15)$$

The system is delocalized for  $a < 1$ ; at the phase transition point  $a = 1$ , it undergoes Anderson localization transition to localized states for  $a > 1$ . This phase transition happens regardless of  $b$ , and in our calculation we set  $b = 1$ . Specially this model is important for us, since by changing parameter  $b$ , we can simulate different models.<sup>41-45</sup> Interestingly, it has similar multi-fractal properties like the Anderson model in three dimensions.<sup>46</sup>

And finally, we also use  $3d$  Anderson model (Eq. (11)) with randomly Gaussian distributed on-site energies,  $\epsilon_i$ , and constant nearest-neighbor hopping amplitudes,  $t = 1$ . The Gaussian distribution has zero mean and variance  $w$ . Anderson phase transition happens at  $w = 6.1$ , with delocalized behavior for  $w < 6.1$  and localized behavior for  $w > 6.1$ .<sup>47</sup>

#### IV. MULTI-FRACTALITY OF MAXIMALLY ENTANGLED MODE

Multi-fractal analysis of Hamiltonian eigen-mode at the Fermi energy  $|E_F\rangle$  has been studied before<sup>19-22,30,31</sup>. Here, fractal properties of MEM is studied and compared with the  $|E_F\rangle$ . To do so, in the following we first inspect profile of MEM in AA model. Then multi-fractal spectrum as well as the singularity spectrum of MEM in PRBA, PRBM, and Anderson  $3d$  are studied. Then, the symmetry relation of the anomalous exponents  $\Delta$ , Eq. (8) for the MEM is verified.

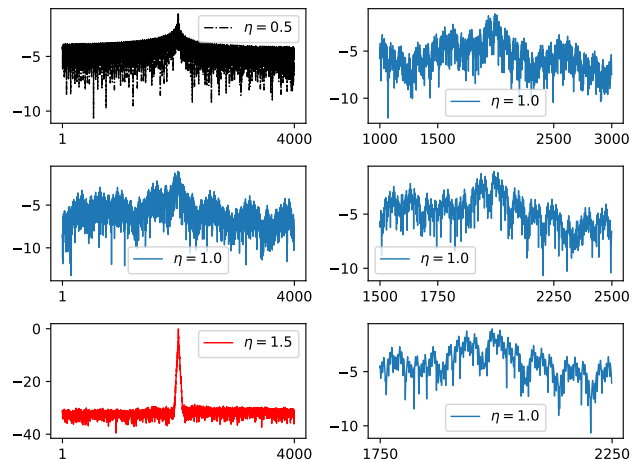


FIG. 1. (color online) Left panels are  $\log_{10} |\psi_i|^2$  of MEM for AA model versus site number for a sample with system size  $N = 4000$  in delocalized phase ( $\eta = 0.5$ , top panel), at the phase transition point ( $\eta = 1.0$ , middle panel), and in the localized phase ( $\eta = 1.5$ , bottom panel). In each of the right panels, a different part of the MEM at the phase transition point is plotted. For each choice, we see the same behavior. Thus MEM at the phase transition point is self-similar. Note that there is no randomness in AA model and we do not have to take disorder average.

#### A. Profile of MEM

First, we look at the profile of MEM in different phases for AA model, which is a disorder-free model and we do not have to take disorder average. We plot MEM in the delocalized phase, localized phase and at the phase transition point in Fig. 1. As we can see, in the delocalized phase, MEM is spread over sites, while it is localized at one site in the localized phase. On the other hand, it shows self-similarity at the phase transition point. i.e. behavior of any part of the MEM is similar to that of the entire mode. Because of such self-similarity, MEM shows multi-fractality.

Moreover, Since fractal properties of eigen-modes are extracted from the GIPR, we compare the GIPR of MEM and  $|E_F\rangle$  according to Eq. (3). GIPR of AA model for different  $q$ 's are plotted in Fig. 2. For each  $q$ , although the behavior is not identical, similar trend is observed. From this simple calculation, we can deduce that MEM has much the same fractal properties as  $|E_F\rangle$ . In addition, similar to the GIPR of the Hamiltonian eigen-mode at the Fermi level, GIPR of the MEM distinguishes different phases and can be used as a phase detection parameter.

#### B. Multi-fractal Spectrum

In this subsection, we consider the behavior of multi-fractal spectrum  $\tau(q)$  as a function of  $q$  for PRBA, PRBM

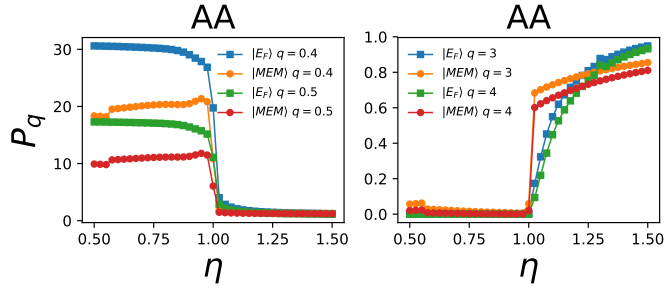


FIG. 2. (color online) Generalized participation ratio, Eq. (3) of both  $|E_F\rangle$  and MEM, for the AA model. Left panel:  $q = 0.4, 0.5$  and Right panel:  $q = 3, 4$ . Both modes have similar behavior in delocalized phase ( $\eta < 1$ ) and in localized phase ( $\eta > 1$ ). System size is  $N = 3000$ . Since there is no randomness in AA model, we do not have to take disorder average.

and Anderson  $3d$  models. In models with randomness, to use Eqs. (5), (9), and (10) we need to take the average of quantities over (quenched) random sample realizations. To do so we can take either ensemble average or typical average. As verified by Ref. [30], typical average yields more accurate results (since very small numbers in  $|\psi_i|^2$  are also take into account). Thus, we only present the results obtained using typical averages. To obtain typical average of GIPR for models with disorder, we rewrite Eq. (5) as:

$$e^{\langle \ln P_q(\lambda) \rangle} \propto \lambda^{\tau(q)^{typ}}, \quad (16)$$

where  $\langle \dots \rangle$  stands for arithmetic average over disorder realization. Thus,

$$\tau(q)^{typ} = \lim_{\lambda \rightarrow 0} \frac{\langle \ln P_q(\lambda) \rangle}{\ln \lambda}. \quad (17)$$

In taking the limit, we are free to either fix  $\ell$  and choose a sequence of system sizes  $N$ , or we can fix  $N$  and choose a sequence of smaller values of cell size:  $1 \ll \ell < N^{26,30,31}$ . Here we choose the former; we choose  $\ell \sim 5$  (for  $1d$  models), and  $\ell \sim 10$  (for  $3d$  model) for  $q < 0$  and  $\ell = 1$  for  $q > 0$  and we increase the system size  $N$ . The reason that we choose  $\ell > 1$  for negative  $q$  is the following: numerical inaccuracies that are the calculated eigen-mode (either for  $|E_F\rangle$  or MEM) become exaggerated for negative  $q$  and thus to avoid them, we coarse grain over a cell with size  $\ell$ . Then, the slope of the straight line fitting  $\langle \ln P_q \rangle$  versus  $-\ln(N)$  gives us the  $\tau(q)$ .

$$-\ln(N) \tau(q)^{typ} = \left\langle \ln \sum_{k=1}^{N_\ell} \mu_k^q \right\rangle, \quad (18)$$

with similar calculations based on Eqs. (9) and (10) we

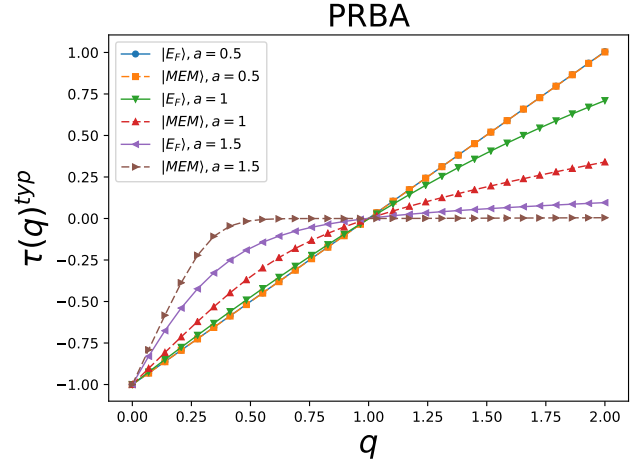


FIG. 3. (color online) Multi-fractality spectrum,  $\tau(q)$  for PRBA. System sizes are between 1000 and 5000 in step of 500. For each data point we averaged over 1000 samples.

obtain  $\alpha$  and  $f(\alpha)$ :

$$-\ln(N) \alpha(q)^{typ} = \left\langle \frac{\sum_{k=1}^{N_\ell} \mu_k^q \ln \mu_k}{P_q} \right\rangle \quad (19)$$

$$-\ln(N) f(q)^{typ} = \left\langle \frac{\sum_{k=1}^{N_\ell} \mu_k^q \ln \mu_k}{P_q} - \ln P_q \right\rangle \quad (20)$$

We know that, multi-fractal spectrum behavior of Hamiltonian eigen-mode  $|E_F\rangle$  depends on the phase of the system: in the delocalized phase,  $\tau(q)$  is a straight line with a constant slope equal to dimension of the system. In the localized phase, the spectrum goes to zero for  $q > 0$ , and at the phase transition point, the slope of the spectrum is not constant, yielding to multi-fractality. The multi-fractal spectrum of MEM and  $|E_F\rangle$  for PRBA, PRBM, and Anderson  $3d$  model are plotted in Fig. 3, Fig. 4, and Fig. 5 respectively. In Fig. 6 disorder averaged  $\langle \ln P_q \rangle$  versus  $-\ln(N)$  plotted and fitted with a straight line for MEM at the phase transition point for PRBA, PRBM, and Anderson  $3d$  models. The slope of this line which is  $\tau(q)$  and the accuracy of the fitted line by R-squared measure are calculated.

In PRBA and PRBM models, the behavior of  $\tau$  in the delocalized phase for both  $|E_F\rangle$  and  $|MEM\rangle$  are identical, both are straight lines; although we see a slight discrepancy behavior for Anderson  $3d$  model. In the localized phase,  $\tau(q)$  goes to zero. And, more importantly at the phase transition point,  $\tau(q)$  is a non-linear function of  $q$ .

We also calculate the fractal dimension of MEM and plot them in Fig. 7. The single fractal dimension of MEM in delocalized phase equals to  $1 = d$  for PRBA and PRBM models, and for Anderson  $3d$  model, it is around  $3 = d$ . For the localized phase, fractal dimension goes to zero as it should. The fractal dimension of MEM at the phase transition point is also plotted, which as we

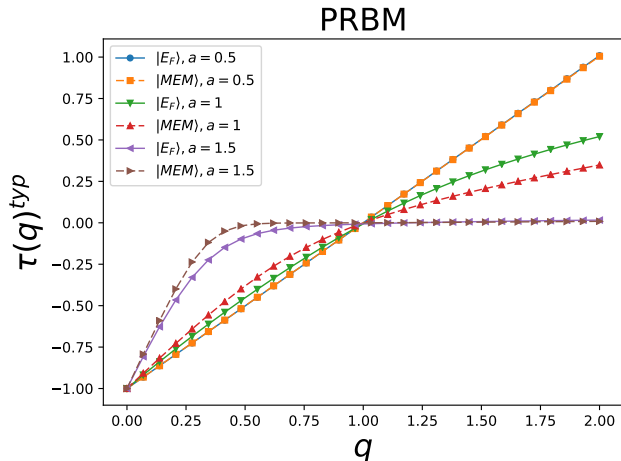


FIG. 4. (color online) Multi-fractality spectrum,  $\tau(q)$  for PRBM. System sizes are between 1000 and 5000 in step of 500. For each data point we averaged over 1000 samples.

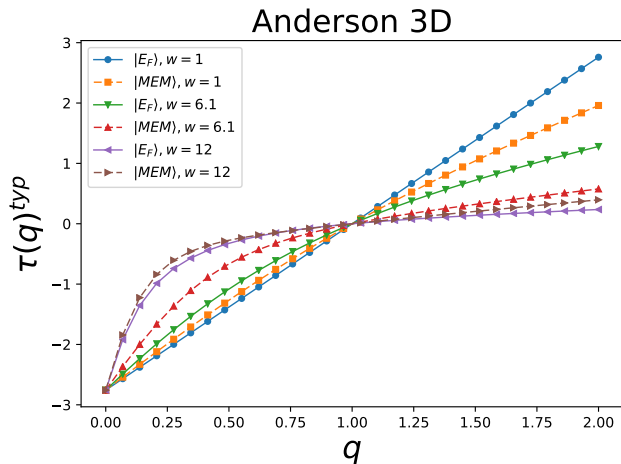


FIG. 5. (color online) Multi-fractality spectrum,  $\tau(q)$  for Anderson  $3d$  model with Gaussian distribution. System sizes are between  $4 \times 4 \times 4$  to  $30 \times 30 \times 30$ , with 300 samples for small sizes and 50 samples for large sizes.

can see, is not a constant and thus MEM is multi-fractal at the phase transition point.

### C. Singularity Spectrum

Next, we consider the behavior of the singularity spectrum  $f(\alpha)$  versus  $\alpha$ . In the delocalized phase,  $f(\alpha)$  should be narrow around  $\alpha = d$ : when the system is delocalized, we expect the eigen-mode (either the eigen-mode of the Hamiltonian or the MEM of entanglement Hamiltonian) to spread over all sites and by the normalization condition  $\sum_{i=1}^{L^d} |\psi_i|^2 = 1$ , we find that  $|\psi_i|^2 \sim L^{-d}$ . Thus, according to Eq. (9),  $f(\alpha)$  should be narrowed

around  $\alpha \sim d$  with the value of  $f(\alpha) \sim d$  (i.e. the fractal dimension of points with  $|\psi_i|^2 \sim L^{-d}$  is very close to the dimension of system  $d$ ). For PRBA and PRBM  $f(\alpha)$  at  $\alpha \sim 1$  is close to 1 and for Anderson  $3d$ ,  $f(\alpha)$  at  $\alpha \sim 3$  is close to 3. At the phase transition point,  $f(\alpha)$  has parabolic behavior<sup>26,30,31</sup> which is the sign of the multi-fractality of the mode. In the localized phase, the eigen-mode is localized at a few number of sites and has a very small value at many other sites, thus  $f(\alpha)$  broadens toward larger  $\alpha$ , i.e. plot is shifted to the right.

Our calculation of singularity spectrum of MEM for PRBA, PRBM, and Anderson  $3d$  is plotted in Fig. 8. According to our calculation, the singularity spectrum of MEM in the delocalized phase is centered around  $\alpha = d = 1$  for PRBA and PRBM models and around  $\alpha = d = 3$  for Anderson  $3d$  model, although it spreads a bit around 3 for the Anderson  $3d$  model. At the phase transition point, we see a parabolic behavior as it is predicted and calculated for Hamiltonian eigen-mode at the Fermi level. And finally, in the localized phase,  $f(\alpha)$  is broadened toward larger  $\alpha$ . We note that  $f(\alpha)$  versus  $\alpha$  is more broadened in the case of Anderson  $3d$  model than in the  $1d$  cases. Beside some inaccuracies that come from two exact diagonalizations to obtain MEM (as we explained in Introduction), we expect more broad behavior for the Anderson  $3d$  case. Since the linear size of the system,  $N$  is the reference in the calculation of  $\alpha$  and  $f(\alpha)$  (see Eqs. (9, 10)), and dimension of the system is three times larger than the  $1d$  cases, thus  $\alpha$  goes to larger values. As we can see, the behavior of the singularity spectrum of MEM like  $|E_F\rangle$  depends on the phase considered, and thus it can be used as a phase detection parameter.

By looking at the Fig. 8, we see that singularity spectrum at the phase transition point for the three studied models are symmetric (in contrast to the results obtained in the Refs. [26 and 46] for PRBM and Ref. [32] for Anderson  $3d$  models, where the reason come from choosing  $\ell > 1$ ). The physics that is behind this symmetry(asymmetry) of  $f(\alpha)$  versus  $\alpha$  which could indicate uniformities (non-uniformities) in the hierarchical organization of mode was pointed out in Ref. [48].

### D. Symmetry Relation of $\Delta_q$

The symmetry relation of anomalous exponents, Eq. (8) is proved analytically and numerically in Refs. [26 and 30] for  $|E_F\rangle$ . Here we present numerical verification of the symmetry relation for the MEM in PRBA, PRBM, and Anderson  $3d$  models in the main panels of Fig. 9. As we can see the symmetry relation of Eq. (8) is respected for the MEM of the entanglement Hamiltonian. On the other hand, we fit the  $\Delta_q$  for the  $|E_F\rangle$  and MEM with the parabolic equation of  $Aq(B - q)$  and find the  $A$  and  $B$  constants. The values of  $A$  and  $B$  are reported in the Table I. For three models considered, and for both  $|E_F\rangle$  and MEM,  $B \sim 1$  as it should be (since  $\tau(1) = 0 \rightarrow \Delta_1 = 0$ , and so  $B = 1$ ). Moreover,  $A_{MEM}$  is approximately

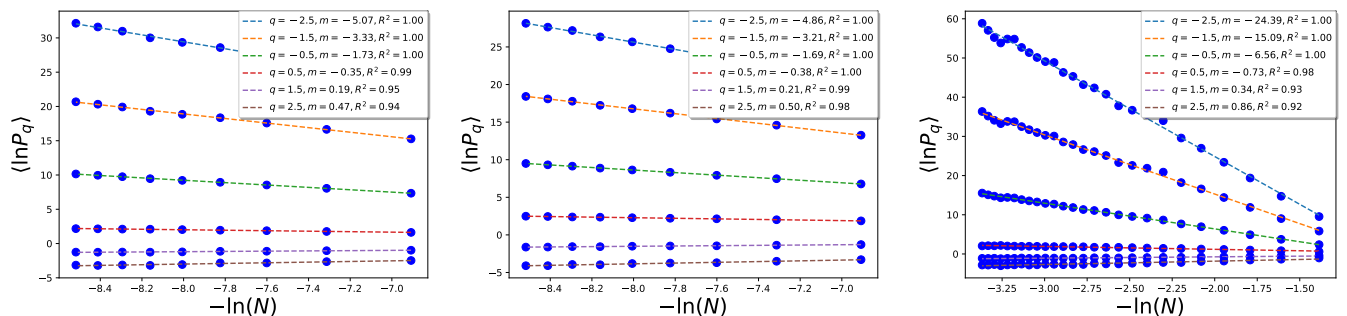


FIG. 6. (color online) Plot of disorder averaged  $\ln P_q$  vs  $-\ln N$  for PRBA(left), PRBM(middle), and Anderson 3d (right) models for the MEM at the phase transition point. This calculation is done for some selected values of  $q$  and for each  $q$  the slope of the fitted line is indicated by  $m$ . The R-squared which is the sign of how close data points are to the fitted line is also calculated (the closer to 1, the better fitted line).

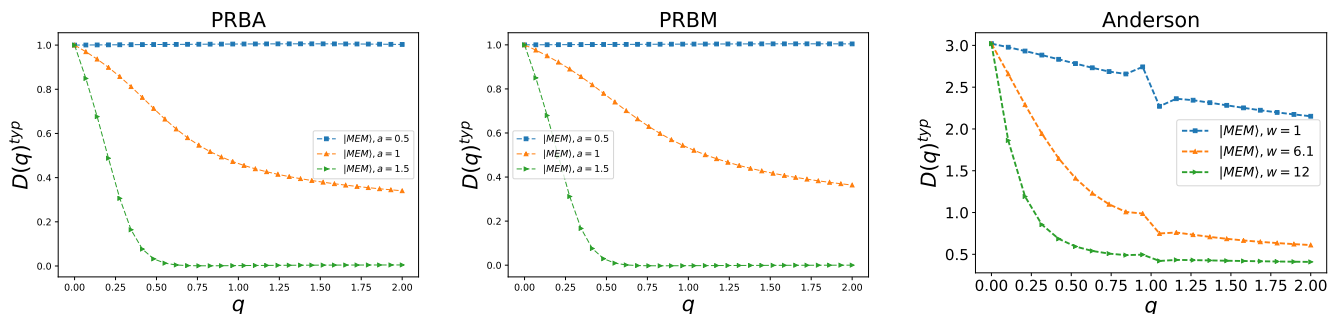


FIG. 7. (color online) Fractal dimension of the MEM of the entanglement Hamiltonian for PRBA (left panel), PRBM (middle panel), and Anderson 3d (right panel) models. For each model, fractal dimension is calculated in delocalized phase, at the phase transition point, and in the localized phase.

three times larger than  $A_{|E_F\rangle}$  in each model.

TABLE I. Constants  $A$  and  $B$  when we fit  $\Delta_q$  for  $|E_F\rangle$  and MEM with the equation  $Aq(B-q)$  (see sub-panels of Fig. 9).

|                   | PRBA    | PRBM    | Anderson 3d |
|-------------------|---------|---------|-------------|
| $A_{ E_F\rangle}$ | 0.11(4) | 0.13(3) | 0.9(5)      |
| $A_{\text{MEM}}$  | 0.4(1)  | 0.35(2) | 2.1(6)      |
| $B_{ E_F\rangle}$ | 0.94(5) | 0.93(3) | 0.9(9)      |
| $B_{\text{MEM}}$  | 1.0(0)  | 0.97(8) | 1.0(7)      |

## V. CONCLUDING REMARKS

It has been shown that Anderson transition as a quantum phase transition exhibits multi-fractal behavior at the critical point. In fact, the generalized participation ratio of Hamiltonian eigen-mode at the Fermi level is a measure that shows multi-fractality of the system. Recently, entanglement Hamiltonian and its associated maximally entangled mode has attracted attention as a tool to characterize systems behavior particularly at the critical point. We note that obtaining an explicit relation for eigenvectors of the entanglement Hamiltonian (EH) based on the eigenvectors of Hamiltonian is not trivial

and they are not directly related. In a study<sup>49</sup>, people found the explicit expression for the EH matrix elements in the ground state of free fermion models. People also found that at the extreme limit of strong coupling between two chosen subsystems, EH of a subsystem and its Hamiltonian are proportional<sup>50</sup>. In this paper, we have shown that multi-fractality of Anderson transition carries over to MEM much in the same way as Hamiltonian eigen-mode at the Fermi level.

Based on numerical calculations for PRBA and PRBM 1d models, and also Anderson 3d model, we showed that single particle MEM of the entanglement Hamiltonian, has the same fractal properties as the Hamiltonian eigen-mode at the Fermi level; although for Anderson 3d model we see a little deviations, since we could not reach very large system sizes. For MEM, in the delocalized phase,  $\tau(q)$  has a slope equal to the dimension of the system, while in the localized phase, it goes to zero. Interestingly, at the phase transition point, MEM is multi-fractal and its multi-fractality is similar to that of the  $|E_F\rangle$ . MEM also follows the symmetry relation of anomalous exponents. Moreover, singularity spectrum  $f(\alpha)$  of MEM, is similar to  $f(\alpha)$  of  $|E_F\rangle$ : in the delocalized phase it is around  $\alpha \sim d$ ; at the phase transition point it has parabolic shape with the maximum value  $d$ , and it broad-



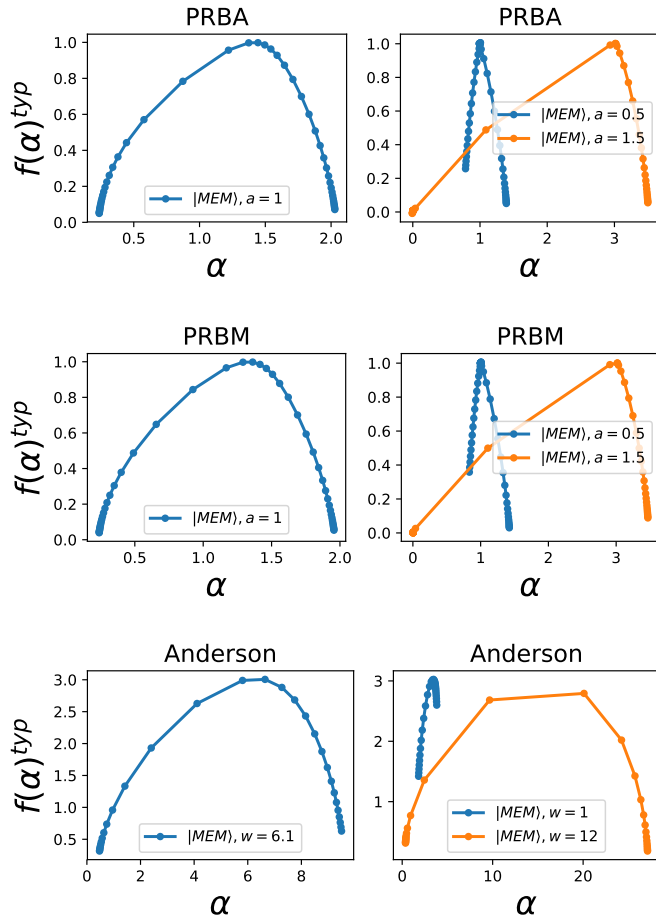


FIG. 8. (color online) Singularity spectrum  $f(\alpha)$  for PRBA, PRBM, and Anderson  $3d$  models. The left panels show the singularity spectrum of MEM at the phase transition point. The right panels show the singularity spectrum of MEM for delocalized and localized phases. For each model, the range of  $q$  is between  $-6$  and  $6$ .

ens in the localized phase. And thus, by looking at multi-fractal spectrum or singularity spectrum of MEM, we can distinguish different phases.

Multi-fractality of an observable at the quantum phase transition means that this observable is self-similar; and finite-size scaling of observable is a legitimate method of obtaining critical exponents. Here we saw that entanglement Hamiltonian shows multi-fractality; which indirectly verifies that reduced density matrix and even entanglement entropy should exhibit self-similarity at the phase transition point, and thus their finite size scaling can be used as a method to calculate the critical exponents, as it has been done in Refs. [51–53].

Multi-fractality of entanglement Hamiltonian was studied in this paper through its eigen-modes. This study could also be done by inspecting the multi-fractality of elements of entanglement Hamiltonian. It might also be interesting to consider entanglement entropy, or a measure of eigenvalues of reduced density matrix, to see if they also carry signatures of multi-fractality.

## VI. ACKNOWLEDGMENTS

This research is supported by University of Mazandaran, National Merit Foundation of Iran, and Institute for Research in Fundamental Sciences (IPM). Part of this work was done while I was working at Shiraz University. I would like to thank Dr. Abbas Ali Saberi and Afshin Montakhab for useful discussions and their constructive criticism on the manuscript.

<sup>1</sup> P. W. Anderson, Phys. Rev. **109**, 1492 (1958).

<sup>2</sup> F. Evers and A. D. Mirlin, Rev. Mod. Phys. **80**, 1355 (2008).

<sup>3</sup> F. Wegner, Z. Phys. B, **36**, 206 (1980).

<sup>4</sup> H. E. Stanley, L. A. N. Amaral, A. L. Goldberger, S. Havlin, P. Ch. Ivanov, C.-K. Peng, Physica A: Statistical Mechanics and its Applications, **270**, 309, (1999).

<sup>5</sup> P. Ch. Ivanov, L. A. N. Amaral, A. L. Goldberger, S. Havlin, M. G. Rosenblum, H. E. Stanley, Z. R. Struzik, Chaos: An Interdisciplinary Journal of Nonlinear Science, **11**, 3, (2001).

<sup>6</sup> A. Davis, A. Marshak, W. Wiscombe, R. Cahalan, Journal of Geophysical Research: Atmospheres, **99**, 8055 (1994).

<sup>7</sup> Y. Tessier, S. Lovejoy, P. Hubert, D. Schertzer, S. Pecknold, Journal of Geophysical Research: Atmospheres, **101**, 26427, (1996). S. Lovejoy, D. Schertzer, Journal of Geophysical Research: Atmospheres, **95**, 2021 (1990).

<sup>8</sup> L. Biferale, G. Boffetta, A. Celani, B. J. Devenish, A. Lanotte, and F. Toschi, Phys. Rev. Lett. **93**, 064502 (2004).

<sup>9</sup> C. Meneveau, K. R. Sreenivasan, Nuclear Physics B, **2**, 0920, (1987).

<sup>10</sup> D. Schertzer et al, Fractals **05**, 427 (1997).

<sup>11</sup> R. R. Prasad, C. Meneveau, and K. R. Sreenivasan, Phys. Rev. Lett. **61**, 74 (1988).

<sup>12</sup> C. Meneveau, K. R. Sreenivasan, P. Kailasnath, M. S. Fan, Phys. Rev. A **41**, 894 (1990).

<sup>13</sup> R. Benzi, G. Paladin, G. Parisi, A. Vulpiani, Journal of Physics A: Mathematical and General, **61**, 3521 (1984).

<sup>14</sup> L. Zunino, B. M. Tabak, A. Figliola, D. G. Perez, M. Garavaglia, O. A. Rosso, Physica A: Statistical Mechanics and its Applications, **387**, 6558 (2008).

<sup>15</sup> K. Matia, Y. Ashkenazy, H. E. Stanley, Europhysics Letters, **61**, 422 (2003).

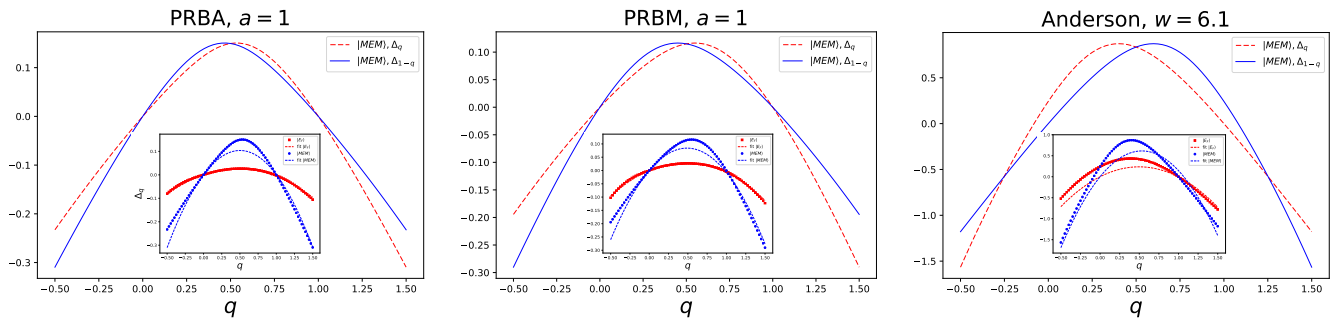


FIG. 9. (color online) Main panels: both  $\Delta_q$  (red) and  $\Delta_{1-q}$  (blue) are plotted to check the symmetry relation  $\Delta_q = \Delta_{1-q}$  for MEM in the PRBA, PRBM, and Anderson  $3d$  models. Sub-panels: fitting  $\Delta_q$  for  $|E_F\rangle$  (red) and MEM (blue) in each model with parabolic equation of  $Aq(B-q)$ . The values of  $A$  and  $B$  for  $|E_F\rangle$  and MEM are reported in Table I.

- 16 X. Sun, H. Chen, Z. Wu, Y. Yuan, Physica A: Statistical Mechanics and its Applications, **291**, 553 (2001).
- 17 P. Oswiecimka, J. Kwapien, S. Drozd, Physica A: Statistical Mechanics and its Applications, **347**, 626 (2005).
- 18 P. Oswiecimka, S. Drozd, J. Kwapien, A. Z. Gorski, Acta Physica Polonica A **117**, 637 (2010).
- 19 A. D. Zdetsis, C. M. Soukoulis, and E. N. Economou, Phys. Rev. B **33**, 4936 (1986).
- 20 C. M. Soukoulis and E. N. Economou, Phys. Rev. Lett. **52**, 565 (1984).
- 21 C. Castellani and L. Peliti, J. Phys. A: Math. Gen. **19** L429 (1986).
- 22 H. Aoki, J. Phys. C **16**, L205 (1983).
- 23 V. I. Fal'ko and K. B. Efetov, Europhysics Letters, **32**, 8 (1995).
- 24 A. Mildenerger and F. Evers, Phys. Rev. B **75**, 041303(R) (2007).
- 25 M. Janseen, Int. J. Mod. Phys. B **8**, 943 (1994).
- 26 A. D. Mirlin, Y. V. Fyodorov, A. Mildenerger, F. Evers, Phys. Rev. Lett. **97**, 046803 (2006).
- 27 X. Jia, A. R. Subramaniam, I. A. Gruzberg, and S. Chakravarty, Phys. Rev. B **77**, 014208 (2008).
- 28 O. Giraud, J. Martin, and B. Georgeot, Phys. Rev. A **79**, 032308 (2009).
- 29 X. Chen, B. Hsu, T. L. Hughes, and E. Fradkin Phys. Rev. B **86**, 134201 (2012).
- 30 L. J. Vasquez, A. Rodriguez, and R. A. Romer, Phys. Rev. B **78**, 195106 (2008).
- 31 A. Rodriguez, L. J. Vasquez, and R. A. Romer, Phys. Rev. B **78**, 195107 (2008).
- 32 A. Rodriguez, L. J. Vasquez, and R. A. Romer, Phys. Rev. Lett. **102**, 106406 (2009).
- 33 I. Klich, Phys. A: Math. Gen. **39**, L85 (2006).
- 34 M. Pouranvari, K. Yang, Phys. Rev. B **89**, 115104 (2014).
- 35 M. Pouranvari, K. Yang, Phys. Rev. B **88**, 075123 (2013).
- 36 M. Pouranvari, K. Yang, Phys. Rev. B **92**, 245134 (2015).
- 37 M. Pouranvari, A. Montakhab, Phys. Rev. B, **96**, 045123 (2017).
- 38 Aubry, S. Andre, G. Ann. Israel. Phys. Soc. **3**, 133 (1980).
- 39 R. P. A. Lima, H. R. da Cruz, J. C. Cressoni, and M. L. Lyra, Phys. Rev. B **69**, 165117 (2004).
- 40 A. D. Mirlin, Y. V. Fyodorov, F. M. Dittes, J. Quezada, and T. H. Seligman Phys. Rev. E **54**, 3221 (1996).
- 41 J. V. Jose and R. Cordery, Phys. Rev. Lett. **56**, 290 (1986).
- 42 A. V. Balatsky and M. I. Salkola, Phys. Rev. Lett. **76**, 2386 (1996).
- 43 B. L. Altshuler and L. S. Levitov, Phys. Rep. **288**, 487 (1997).
- 44 I. V. Ponomarev and P. G. Silvestrov, Phys. Rev. B **56**, 3742 (1997).
- 45 G. Casati and T. Prosen, Physica D **131**, 293 (1999); F. Borgonovi, P. Conti, D. Rebuszi, B. Hu, and B. Li, Physica D **131**, 317 (1999).
- 46 A. D. Mirlin and F. Evers, Phys. Rev. B **62**, 7920 (2000).
- 47 P. Markos, Acta Physica Slovaca. Reviews and Tutorials. **56**, 561 (2010).
- 48 S. Drozd and P. Oswiecimka, Phys. Rev. E **91**, 030902(R) (2015).
- 49 V. Eisler and I. Peschel, Journal of Physics A: Mathematical and Theoretical **50**, 284003 (2017).
- 50 I. Peschel and M. C. Chung, EPL (Europhysics Letters) **96**, 50006 (2011).
- 51 A. Zhao, R. L. Chu, S. Q. Shen, Phys. Rev. B **87**, 205140 (2013).
- 52 F. Igloi and Y. Lin, J. Stat. Mech. (2008) P06004.
- 53 Y. Wang, T. Gulden, A. Kamenev, Phys. Rev. B **95**, 075401 (2017).